



HAL
open science

Influence of environmental changes on the biogeochemistry of arsenic in a soil polluted by the destruction of chemical weapons: A mesocosm study

Hugues Thouin, Fabienne Battaglia-Brunet, Marie-Paule Norini, Lydie Le Forestier, Mickael Charron, Sébastien Dupraz, Pascale Gautret

► To cite this version:

Hugues Thouin, Fabienne Battaglia-Brunet, Marie-Paule Norini, Lydie Le Forestier, Mickael Charron, et al.. Influence of environmental changes on the biogeochemistry of arsenic in a soil polluted by the destruction of chemical weapons: A mesocosm study. *Science of the Total Environment*, 2018, 627, pp.216-226. 10.1016/j.scitotenv.2018.01.158 . insu-01700628

HAL Id: insu-01700628

<https://insu.hal.science/insu-01700628v1>

Submitted on 12 Feb 2018

HAL is a multi-disciplinary open access archive for the deposit and dissemination of scientific research documents, whether they are published or not. The documents may come from teaching and research institutions in France or abroad, or from public or private research centers.

L'archive ouverte pluridisciplinaire **HAL**, est destinée au dépôt et à la diffusion de documents scientifiques de niveau recherche, publiés ou non, émanant des établissements d'enseignement et de recherche français ou étrangers, des laboratoires publics ou privés.

Influence of environmental changes on the biogeochemistry of arsenic in a soil polluted by the destruction of chemical weapons: a mesocosm study

Hugues Thouin ^{a,b,c,d}, Fabienne Battaglia-Brunet ^{a,b,c,d}, Marie-Paule Norini ^{b,c,d}, Lydie Le Forestier ^{b,c,d}, Mickael Charron ^a, Sébastien Dupraz ^a and Pascale Gautret ^{b,c,d}

^a BRGM, 3 avenue Claude Guillemin, 45060 Orléans, France

^b Université d'Orléans, ISTO, UMR 7327, 45071 Orléans, France

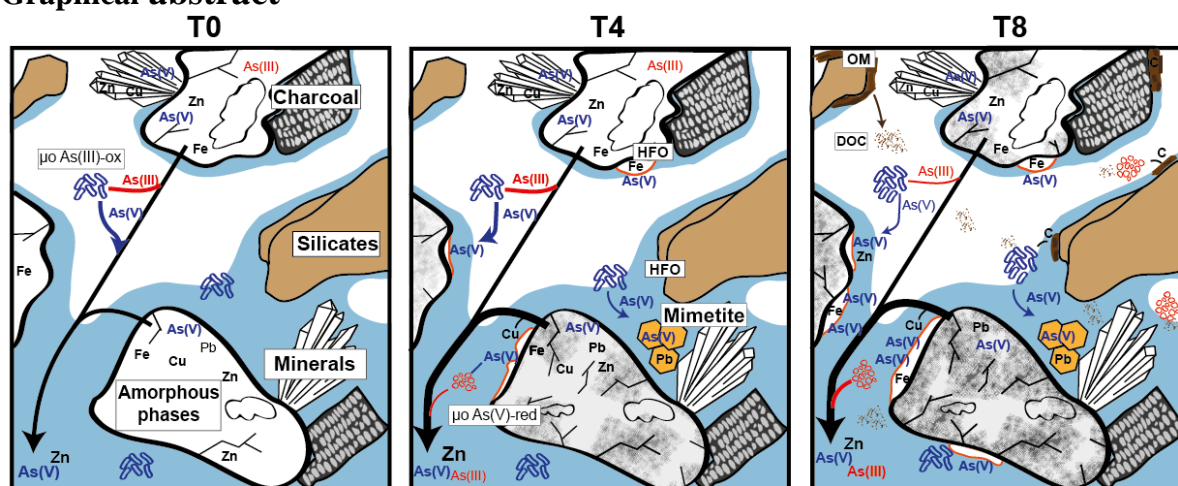
^c CNRS, ISTO, UMR 7327, 45071 Orléans, France

^d BRGM, ISTO, UMR 7327, BP 36009, 45060 Orléans, France

Highlights

- The surface of the main As, Cu and Zn carrier was altered in water saturated conditions
- Precipitation of As(V)-bearing mineral mimetite contributed to the immobilization of As and Pb
- The addition of OM contributed to the growth of As transformation microorganisms
- As(III)-oxidizing activity was decreased by OM but remained the major As transformation phenomenon in the system.

Graphical abstract



Abstract

Thermal destruction of chemical munitions from World War I led to the formation of a heavily contaminated residue that contains an unexpected mineral association in which a microbial As transformation has been observed.

A mesocosm study was conducted to assess the impact of water saturation episodes and input of bioavailable

organic matter (OM) on pollutant behavior in relation to biogeochemical parameters. Over a period of about eight (8) months, the contaminated soil was subjected to cycles of dry and wet periods corresponding to water table level variations. After the first four (4) months, fragmented litter from the nearby forest was placed on top of the soil. The mesocosm solid phase was sampled by three rounds of coring: at the beginning of the experiment, after four (4) months (before the addition of OM), and at the end of the experiment. Scanning electron microscopy coupled to energy dispersive X-ray spectroscopy observations showed that an amorphous phase, which was the primary carrier of As, Zn, and Cu, was unstable under water-saturated conditions and released a portion of the contaminants in solution. Precipitation of a lead arsenate chloride mineral, mimetite, in soils within the water saturated level caused the immobilization of As and Pb. Mimetite is a durable trap because of its large stability domain; however, this precipitation was limited by a low Pb concentration inducing that high amounts of As remained in solution. The addition of forest litter modified the quantities and qualities of soil OM. Microbial As transformation was affected by the addition of OM, which increased the concentration of both As(III)-oxidizing and As(V)-reducing microorganisms. The addition of OM negatively impacted the As(III) oxidizing rate, however As(III) oxidation was still the dominant reaction in accordance with the formation of arsenate-bearing minerals.

Keywords: Arsenic, metal, mineral stability, microbial arsenic transformation, organic matter, dry/wet cycles, mesocosm study

1 **1. Introduction**

2 At the end of the First World War (1914-1918), the former combatants had large stockpiles of unfired munitions.
3 These unspent weapons were dismantled to recycle reusable material, then destroyed or abandoned by ocean
4 dumping or land burial. Chemical weapons containing nitroaromatic, chlorine, bromine or arsenical compounds
5 were destroyed primarily by burning because of their hazardous nature. The site called “Place-à-Gaz”, located
6 northeast of Verdun (France), is one of many sites along the western front line where chemical shells were
7 destroyed. Between 1920 and 1928, approximately 200,000 shells containing organo-arsenic compounds were
8 subjected to simple thermal treatment (Bausinger et al., 2007). The burnt munitions were primarily “blue cross
9 shells” filled with arsenic-bearing vomiting agents CLARK I (diphenylchloroarsine) and CLARK II
10 (diphenylcyanoarsine).

11 Thermal treatment resulted in severe As and heavy metal contamination of the upper 10 - 40 cm of topsoil at the
12 site (Bausinger et al., 2007; Thouin et al., 2016). The surface layer where the inorganic contaminants are
13 concentrated corresponds to the combustion residues of the munitions. This layer, composed of slag, scoria, various
14 munitions elements, and large amounts of ash and charcoal from the firewood used for burning, is black in color
15 (Bausinger et al., 2007; Thouin et al., 2016). The central part of the site was heavily contaminated with As, Zn,
16 Cu, and Pb; concentrations of these elements reached 72,820 mg.kg⁻¹, 90,190 mg.kg⁻¹, 9,113 mg.kg⁻¹ and
17 5,777 mg.kg⁻¹, respectively (Thouin et al., 2016). Most organo-arsenic agents/compounds were oxidized during
18 combustion, resulting in the release of inorganic arsenic As₂O₃ and As₂O₅ (Bausinger et al., 2007). A previous
19 study by Thouin et al., (2016) showed that As was principally present as the pentavalent form (As(V)) within the
20 solid phases (about 98 % of arsenate and 2 % of arsenite (As(III))) and that several arsenate minerals (adamite-
21 olivenite series and pharmacosiderite) crystallized as the material cooled. An amorphous phase rich in Fe, Zn, Cu,
22 and As and presenting a vitreous texture was also observed, highlighting the association of this unusual mineral
23 assemblage with thermal treatment.

24 Microorganisms actively contributing to the metabolism of carbon and arsenic were detected at the site despite
25 low organic matter (OM) bioavailability (Thouin et al., 2016). Microbial activity plays a major role in As
26 speciation in soils (de Mello et al., 2007; Yamamura et al., 2009). For example, in mining environment, microbial
27 As-transforming activity was used in biomining of As-bearing minerals and to clean up post mining contamination
28 (Drewniak and Sklodowska 2013). Several bacterial mechanisms are responsible for As(III) oxidation or As(V)

29 reduction (Battaglia-Brunet et al., 2002; Bachate et al., 2012; Zobrist et al., 2000; Stolz et al., 2002), thus driving
30 As mobility and bioavailability. Changes in environmental conditions, such as modifications of Eh or pH, are
31 likely to modify these microbial activities. Moreover, the concentration and the composition of soil OM affect a
32 microorganism diversity and biomass (Tiedje et al., 1999) and may impact bacterial As transformation (Bachate
33 et al., 2012; Lescure et al., 2016). The cyclic saturation of soils was shown to induce the mobility and change of
34 speciation of arsenic in relation with bacterial activities. Fe and As reduction and release were observed during
35 flooding of contaminated soil (Weber et al., 2010) or redox oscillations (Couture et al., 2015). As-transforming
36 microbes contribute actively to the transformation of As species in frequently saturated soils such as paddy fields
37 (Xiao et al., 2016). However, up to now, the activity of As(III)-oxidizing and As(V)-reducing microorganisms has
38 not been evaluated in highly polluted environments presenting the particular structure and composition of the
39 weapon burning sites, and submitted to fluctuating water regimes.

40 The contaminated soil at the “Place-à-Gaz” site is regularly subjected to partial water saturation during periods of
41 high precipitation and runoff because of the underlying clayey formation. Moreover, the margin of the site near
42 the oak forest is exposed to natural deposition of litter that provides bioavailable OM. These environmental
43 variations are capable of altering the carriers phases of As and affect bacterial As transformation activities, thereby
44 changing As mobility at the site.

45 With the aim to better understand the cycle of As in this highly polluted material submitted to environmental
46 changes, an eight-month experiment was performed in a 1 m³ mesocosm filled with contaminated material that
47 was subjected to water saturation episodes and input of bioavailable OM. Monitoring of interstitial water
48 composition at different/various depths in the mesocosm and of leachate (outlet water) provided information on
49 the processes that affect the fate of As and other inorganic contaminants and their transfer towards surrounding
50 environmental compartments (Thouin et al., 2017). After Zn, As was the most mobile inorganic contaminant in
51 the soil water, with concentrations ranging from 20 to 110 µM. The present study was focused on the evolution of
52 the solid compartment: mineral phases and arsenic-associated microbial parameters. The goal work was to analyze
53 changes in mineral phases and variations in arsenic-associated microbial parameters to increase our understanding
54 of the As cycle in this highly-polluted material that is undergoing environmental exposure.

55

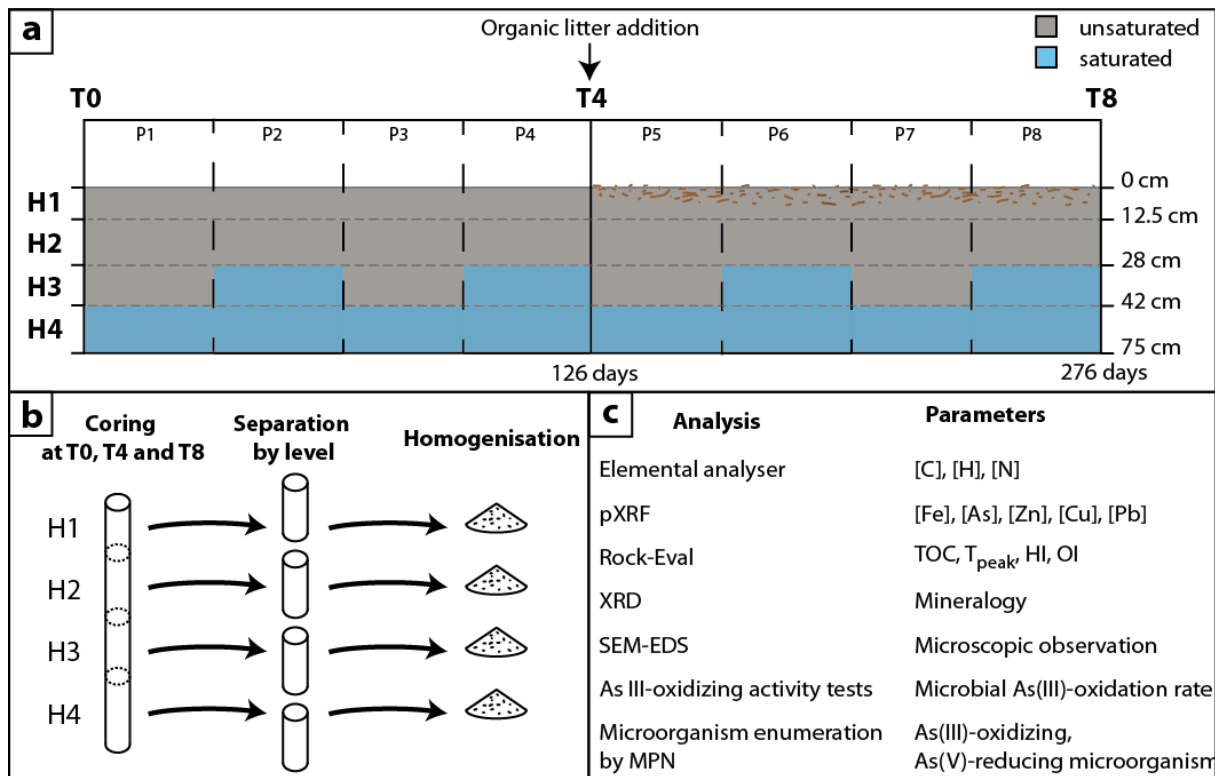
56

57 **2. Materials and methods**

58 **Experiment and soil sampling**

59 Soil was collected at the site named “Place-à-Gaz” (Spincourt Forest, 20 km from Verdun, France) and
60 characterized by Bausinger et al. (2007) and Thouin et al. (2016). It contains slag, coal ash, and residues from
61 ammunition resulting in high concentrations of Zn, As, Cu, and Pb and high organic content (25.9 %).

62 All soil samples described here come from the instrumented mesocosm experiment presented in Thouin et al.
63 (2017) and shown in supplementary material (SM1). Water and solute fluxes of polluted soil were monitored for
64 276 days using the experimental device, which consisted of a closed stainless steel column (1 m in diameter and
65 120 cm high), filled with 610 kg of homogenized contaminated soil. After three months of stabilization, the soil
66 was subjected to dry/wet cycles (over a period of about eight (8) months) and to the addition of organic forest litter
67 at the top of the surface soil at the midpoint of the experiment (after four (4) months at T4)(Fig.1.a). The dry period
68 was characterized by a saturation limited to the mesocosm bottom, and by the addition of around 12 L of Mont
69 Roucous mineral water once a week. The wet period was characterized by the elevation of the water level and by
70 the addition of 6 L of water every two days. Rainfall was simulated by a sprinkler system. In order to obtain the
71 data previously presented in Thouin et al. (2017), soil solution was sampled at four sampling levels (H1, H2, H3
72 and H4; Fig.1.a) thanks to inert porous probes. H1 and H2 levels were permanently unsaturated, H4 level was
73 permanently saturated and H3 level was not saturated during dry periods but was saturated during wet periods.



74

75 **Fig.1.** a. Experiment design. P1, P3, P5, P7 and P2, P4, P6, P8 were respectively dry and wet periods. From the
 76 beginning of P5 forest litter was added at the top of the contaminated soil. H4 was permanently saturated; H2 and
 77 H1 were never saturated. The H3 level was not saturated in the dry periods and saturated in the wet periods
 78 (modified from Thouin *et al.*, 2017). b. Coring and sampling of solid material at T0 (at the beginning of the
 79 experiment), T4 (after 4 months just before the addition of organic litter) and T8 (at the end of this experiment,
 80 i.e. after 8 months). c. Analytical methods and associated parameters performed on each soil sample.

81 Coring was performed in the mesocosm using 5 cm diameter stainless steel pipes, at three steps of the experiment:
 82 at the beginning (T0), before the addition of fragmented forest litter at the end of month 4 (T4), and at the end of
 83 month 8 (T8). After sampling, the pipes were clogged and put back in place in the soil to fill the empty space. Each
 84 core was separated into four samples, H1 at a depth of 0-12.5 cm, H2 at 12.5-28 cm, H3 at 28-42 cm, and H4 at
 85 42-75 cm, corresponding to the soil water sampling levels (Fig.1.b). These samples were homogenised and
 86 collected in sterile glass jars that were tightly closed and stored at 5°C.

87 Analytical techniques

88 For chemical analyses, soil samples were dried and ground to 70 µm. Total carbon, nitrogen, and hydrogen were
 89 quantified in powdered samples, using an elemental flash pyrolyser analyser (Flash 2000, Thermo Fischer
 90 Scientific). Total organic carbon (TOC), hydrogen index (HI), oxygen index (OI), and maximum temperature
 91 of pyrolysable OM (T_{peak}) were determined by Rock-Eval pyrolysis (Rock-Eval 6 Turbo, Vinci Technologies).
 92 The operating principles of this apparatus are described in Lafargue *et al.* (1998). HI can be used as a maturation

93 indicator and is calculated from the amounts of hydrocarbons generated through thermal cracking of nonvolatile
94 organic matter relative to the amount of organic carbon. OI represents the amount of hydrogen relative to the
95 amount of organic carbon present in a sample. It is calculated from the amount of CO₂ and CO released during
96 pyrolysis of the sample. T_{peak} is the accurate temperature experienced by the sample when producing the maximum
97 amount of hydrocarbons. Total concentrations of As, Cu, Zn, Pb, and Fe were determined using an XL3t800
98 NITON[®] portable X-ray fluorescence field apparatus (pXRF). The correct correlation of the metal
99 concentrations determined by this technique and by ICP-MS was previously checked in the same soil (Thouin
100 et al., 2016).

101 The mineralogical composition of the bulk samples was determined by powder X-ray diffraction (XRD). XRD
102 patterns were recorded using an INEL CPS120 diffractometer montage transmission (Debye-Scherrer geometry)
103 equipped with a Co anode (Co K α_1 = 1.78897 Å) and operating at 35 kV and 35 mA. Scans were recorded from
104 5° to 90° (2 θ) with angular steps of 0.03° and a total acquisition time of 210 min.

105 Scanning electron microscopy (SEM) and energy dispersive X-ray spectroscopy (EDS) were used to study the
106 structural evolution of As and metal carrier phases during the experiment and to identify possible new precipitated
107 phases. The samples were air dried, deposited on a carbon adhesive and directly analyzed. All types of grains were
108 investigated for morphological observation and elemental distribution. SEM was performed on a TM 3000
109 (Hitachi) operating at 15 kV accelerating voltage. The SEM was coupled to a Swift ED 3000 X-Stream module
110 (Hitachi). The acquisition time of EDS point analyses was 300 seconds.

111 **As(III)-oxidizing activity tests and bacterial enumeration**

112 Soil samples were incubated at 25°C for 72 h before starting the As(III)-oxidizing activity tests and the
113 enumeration of As(III)-oxidizing and As(V)-reducing microorganisms. It was previously shown that this step
114 allows restoring As-related microbial activities in soil and sediment samples that were stored at 5°C (Lescure et
115 al., 2013; 2016). The As(III)-oxidizing tests were performed in triplicate in 250 mL Erlenmeyer flasks filled with
116 100 mL of CAsO1 medium (Bachate et al., 2002) supplemented with 1 mM As(III) and inoculated with a mass of
117 material equivalent to 0.2 g of dry weight. Flasks were plugged with cotton to retain oxidizing conditions and were
118 incubated at 25° under agitation (100 rpm). Samples were filtrated (0.45 μ m) and stored at -20°C until analysis.
119 As(III) and As(V) were separated using the PDC/MIBK method (Battaglia-Brunet et al., 2002). Separated neutral
120 fraction, attributed to As(V) was then quantified by Flame Atomic Absorption Spectrometry (FAAS) (Varian, Palo

121 Alto, CA, USA). As(III)-oxidizing rates were determined by linear regression fitting of the As(V) concentration
122 versus time line, during the reaction.

123 The evolution of the concentration in As(III)-oxidizing and As(V)-reducing microorganisms was followed using
124 the Most Probable Number method (MPN). The method for As(III)-oxidizing microorganisms is detailed in
125 Thouin et al. (2016). For As(V)-reducing microorganisms (method adapted from Kuai et al., 2001), fresh soil
126 (equivalent to 0.2 g dry soil) was placed in a sterile, glass Erlenmeyer flask with 10 mL of sterile physiological
127 saline (9 g.L⁻¹ NaCl in demineralized water), shaken for 30 min at 25°C, then sonicated 2 x 20 s at 45 kHz.
128 Triplicate suspensions were prepared for each sample. Soil suspensions were diluted in sterile physiological saline
129 solution to a dilution of 10⁻⁶. CAsO1 basal mineral medium (Battaglia-Brunet et al., 2002) was complemented with
130 20 mM lactic acid and As(V) (100 mg.L⁻¹). The medium was distributed over Microtest TM Tissue culture plates
131 (96 wells), 250 µL per well. Each well was inoculated with 25 µL of diluted soil suspension. Five wells were
132 inoculated with each dilution. Culture plates were incubated at 25°C for 10 days in anaerobic jars with Anaerocult
133 packs (Merck). The presence of As(III) formed in the wells during incubation was revealed by the formation of
134 As(III)-PyrrolidineDithioCarbamate (PDC), an insoluble white complex: 80 µL of 0.1 M acetate buffer (pH 5) and
135 40 µL PDC solution (5 g.L⁻¹) were added to each well. The number of positive wells for each dilution was
136 determined, and the most probable number of As(V)-reducing microorganisms was given by the Mc Grady table
137 for five tubes.

138 **Statistical analyses**

139 Statistical tests were carried out using R 3.2.4 (www.r-project.org). Pearson correlations were calculated with the
140 four soil samples at three time steps *i.e.* 12 observations. Principal component analysis (PCA) was performed on
141 biogeochemical parameters on the same observations.

142 **3. Results and discussion**

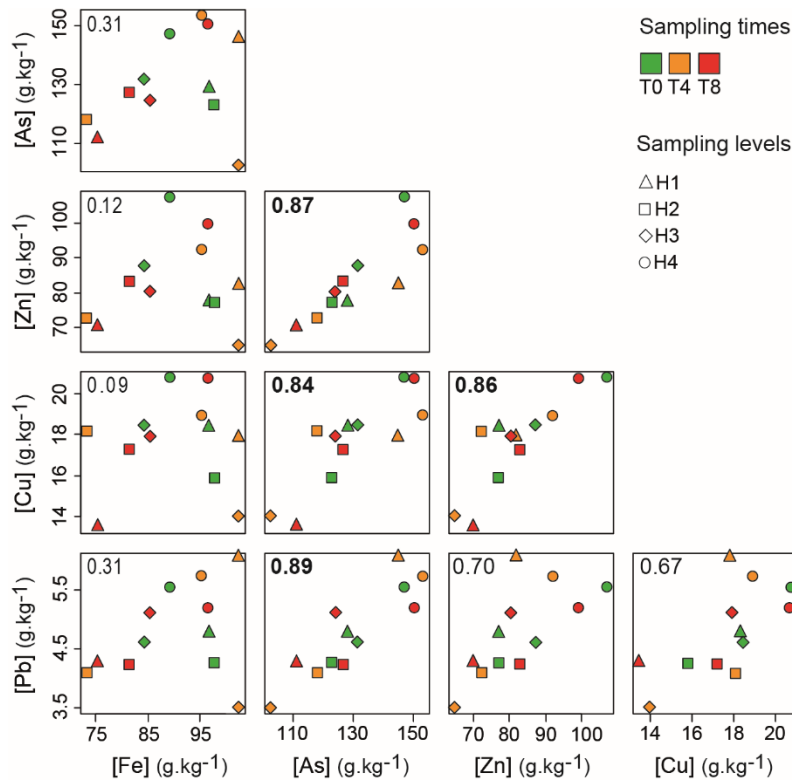
143 **3.1. Stability of As bearing mineral phases**

144 **Relationship between As and metals**

145 As and metal concentrations measured/quantified by the pXRF method were high in all soil samples, in the
146 following decreasing order As > Fe > Zn > Cu > Pb (SM2). Arsenic concentrations ranged from 102,380 to 150,360
147 mg.kg⁻¹, Zn concentrations from 70,040 to 107,400 mg.kg⁻¹, Cu concentrations from 13,450 to 20,790 mg.kg⁻¹,
148 and Pb concentrations from 3,490 to 6,030 mg.kg⁻¹ (SM2). These inorganic contaminant concentrations were very
149 elevated and in the same range as those measured in other soil samples from the same site (Bausinger et al., 2007;

150 Thouin et al., 2016). Concentration variations were difficult to detect with depth and time because of the high
151 heterogeneity of the soil. However, at the end of the experiment (T8), metal(loid) concentrations seemed to be
152 distributed in a pattern showing higher values at the bottom of the mesocosm (H4) (Fig.2; SM2). Moreover, As
153 and metals were less concentrated at the surface after eight (8) months than at the beginning of the experiment
154 (Fig.2; SM2). These observations may be the result of the downward vertical transport of metals within the
155 mesocosm and their accumulation in the saturated soil. Monitoring of metal(oid) concentrations in interstitial water
156 (Thouin et al., 2017) showed that As was immobilized in the bottom level H4 of the mesocosm as its concentration
157 values decreased from 60-80 μM in unsaturated soil to 40 μM in the saturated zone. However, this phenomenon
158 was not observed with other inorganic contaminants. Moreover, the amounts of As released from the liquid phase
159 in the saturated parts are too low to explain the increase of about 40,000 mg.kg^{-1} at the bottom of the mesocosm.
160 It seems more likely that these results highlight the downward particular transport of contaminant-bearing fine
161 particles during the experiment, even if these results are not sufficient to confirm this hypothesis.

162 Arsenic concentration was significantly correlated with that of metals, as shown by Pearson indices > 0.80 (Fig.2),
163 with the exception of Fe concentration which was not correlated with any other metal(loid)s. These results suggest
164 that As, Zn, Cu, and Pb were mainly linked to the same solid phase, as shown in previous characterizations of the
165 polluted material (Thouin et al., 2016), indicating that the principal As carrier was an amorphous phase containing
166 high concentrations of metals.



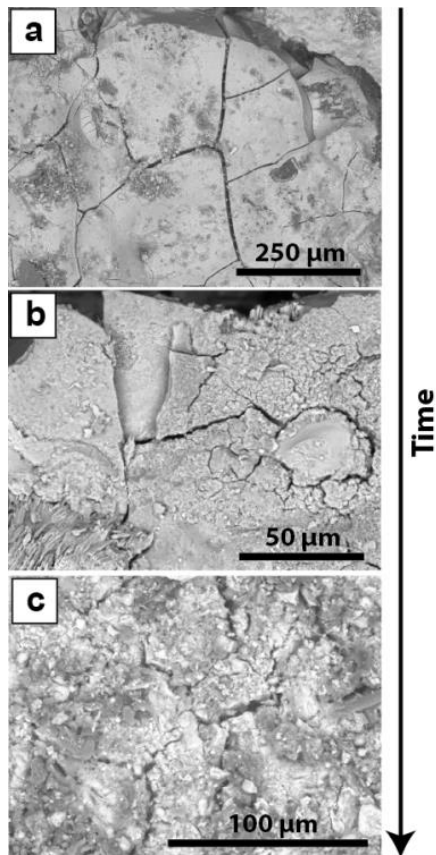
167

168 **Fig.2.** Scatterplot matrix of metal(loid) concentration. Pearson correlation coefficient of variables is specified in
 169 the upper-left corner of each panel (highest correlations are indicated in bold characters).

170 **Stability of amorphous phases**

171 Morphological evolution of amorphous phases was observed by SEM in various samples, so as to compare their
 172 stability at different times and under different environmental conditions. In the unsaturated levels, amorphous
 173 phases did not show evidence of weathering all along the experiment. Figure 2 shows the textural evolution of the
 174 vitrified amorphous phases in the soil level that was permanently water saturated. At the beginning of the
 175 experiment (Fig.3 (a)), this phase was characterized by a smooth texture with micro-cracks, similar to the
 176 morphology previously observed in samples from the site and attributed to the thermal process used to destroy the
 177 weapons (Thouin et al., 2016). After four (4) months of the mesocosm experiment, the surface of the amorphous
 178 phases had changed and taken on a rough texture (Fig.3 (b)). Edges of the cracks were altered and new fissure
 179 networks grew from the previous micro-cracks. At the end of the experiment, after 276 days of water saturation,
 180 the fissure networks covered the entire surface of the amorphous phases, which had become highly irregular (Fig.3
 181 (c)). Similar observations have been made during the alteration of a partially vitrified metallurgical waste (Seigneur
 182 et al., 2007). This morphological evolution may be consistent with dissolution of amorphous phase surfaces in the
 183 saturated soil, which should be accompanied by the release of As, Zn, Cu, Pb. However, metal(oid)s behaved

184 differently with high As and Zn concentrations in solution, whereas Cu, Pb and Fe were not very mobile (Thouin
185 et al., 2017).



186

187 **Fig.3.** Backscattered electron images of amorphous phases in the saturated soil. (a), (b) and (c) illustration of three
188 amorphous phases sampled in the H4 level at T0, T4 and T8 respectively.

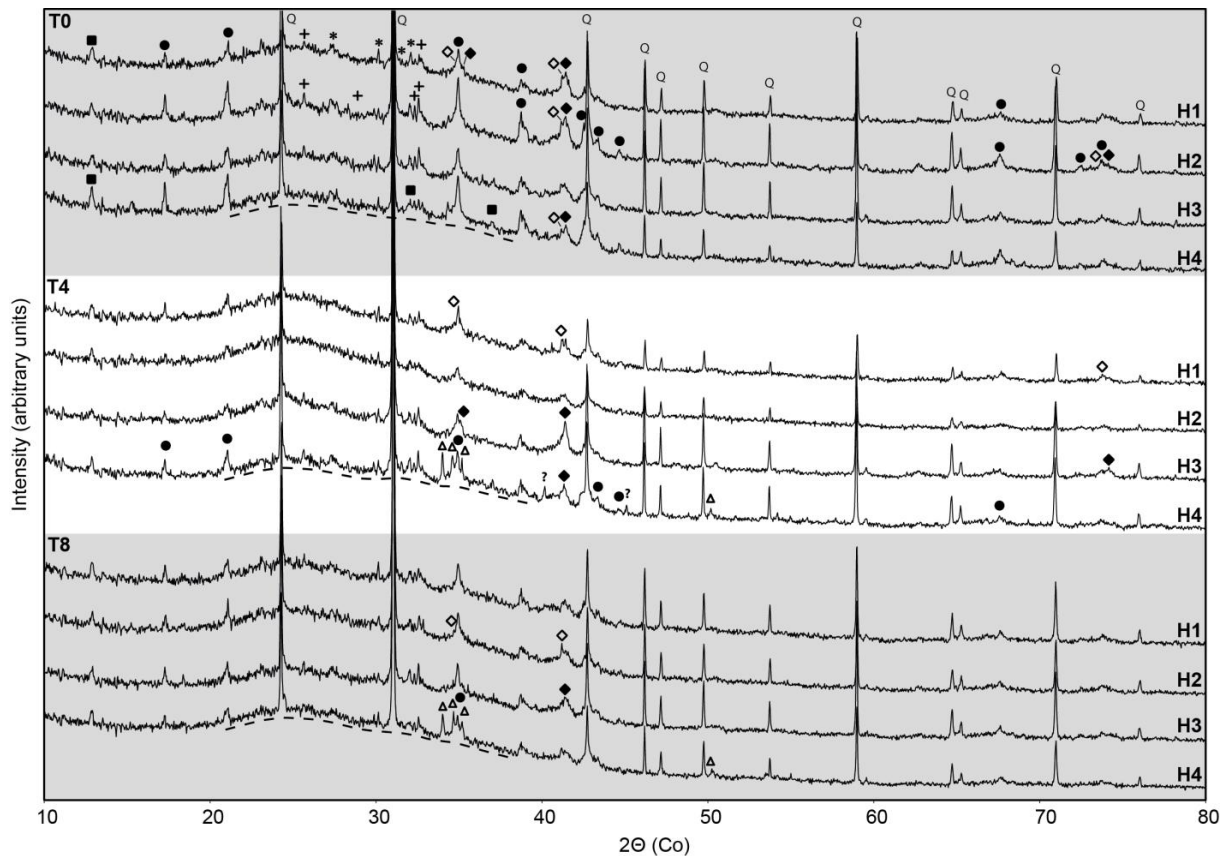
189 Elemental composition of altered amorphous phases was investigated using SEM-EDS analyses (SM3). The
190 elemental maps of Fe, Zn, As, Pb and Cu on amorphous phases presenting a partially altered surface showed a
191 different distribution between Fe and Zn. In this study zone Fe content was lower in the smooth amorphous phases
192 than in the rough surface. An alteration study of partially vitrified metallurgical waste composed primarily of an
193 iron-silica-lime glass matrix showed that altered glass is characterized by relative enrichments of iron induced by
194 high calcium depletion (Seigneur et al., 2007). Here the results were similar, with higher iron concentrations in
195 altered material even though this amorphous material does not have the same chemical composition (no silicium).
196 Other studies showed that under oxidizing conditions, iron mobilized during dissolution of the vitrified material
197 precipitated on the surface of the altered zone (Deneele 2002; Ettler et al., 2004). Our results can be explained by
198 the precipitation of amorphous and poorly crystallized ferric oxides and/or hydrous ferric oxides (HFO) in the
199 proximity of the amorphous phase, which can bind a portion of As and metals. This hypothesis is consistent with
200 the low concentrations of mobile Fe ($< 40 \mu\text{M}$ throughout the experiment, Thouin et al., 2017). The precipitation

201 of iron oxy-hydroxide permits the sorption of Cu and Pb (Swallow et al., 1980) and may also explain the low
202 mobility of these elements. Moreover, the high adsorption of As(V) by amorphous HFO is a well-known
203 phenomenon (Dixit and Hering 2003). Thus, precipitation of HFO resulting from the dissolution of amorphous
204 phases in the water-saturated material may be one of the phenomena inducing the immobilization of As(V) that
205 was observed in this specific environment of the mesocosm. The Zn depletion observed in the surface of the altered
206 zone (SM3) seems to show the easier mobilization and the low affinity to HFO of Zn. These assumptions are
207 consistent with the important Zn concentration in the soil solution, induced by favorable pH conditions (pH range
208 of 5-6; Thouin et al., 2017), during the experiment.

209 **Evolution of the mineralogical association**

210 XRD analysis of soil samples from different depths was used to investigate the mineralogical evolution of the
211 polluted material during the experiment (Fig.4). First, the high background of X-ray diffractograms confirmed the
212 abundance of amorphous phases in the soil. Quartz and potassium and sodium feldspars were identified in each
213 sample with a relative peak intensity that evolved slightly over time and depth. These silicates, which had already
214 been observed in samples from the polluted site (Thouin et al., 2016), were attributed to the substrate, *i.e.* the
215 clayey Woëvre formation.

216 Magnetite (Fe_3O_4) and franklinite (ZnFe_2O_4) were detected in most samples. Magnetite and franklinite exhibit a
217 spinel structure with similar lattice parameters that result in an overlapping of their corresponding XRD peaks, so
218 it is difficult to ascertain the presence of franklinite with XRD spectra. However, the Zn concentration in solids
219 and the common occurrence of the magnetite-franklinite mineral association in metallurgical furnace wastes
220 (Pisciella et al., 2001; Juillot et al., 2003; Dutra et al., 2006; Puziewicz et al., 2007; Seignez et al., 2007; Vereš
221 2014) and in vitrified products of electrostatic precipitator ash from municipal solid wastes (Le Forestier and
222 Libourel 2008) suggest that magnetite-franklinite solid solutions are present as a result of the thermal destruction
223 process. The presence of zincite in site soil samples (Thouin et al., 2016) and in metallurgical wastes, together
224 with magnetite and franklinite (Dutra et al., 2006; Puziewicz et al., 2007; Vereš 2014), confirm the inherited
225 character of these minerals in this context. Although not detected by XRD in the mesocosm samples, zincite, as
226 well as magnetite and franklinite, were most probably present but in insufficient amounts for appropriate detection
227 due to soil heterogeneity. No significant effect of dry/wet cycles or the addition of OM on the stability of these Fe
228 and Zn minerals was detected.



229

230 **Fig.4.** X-ray diffractograms of bulk soil samples. Q: quartz (ICDD-1045); * : sodium feldspar (ICDD 19-1184);
 231 + : potassium feldspar (ICDD 31-0966); ● :adamite (ICDD 39-1354); ■ :Na-Pharmacosiderite (ICDD 38-0388);
 232 ◆ : magnetite (ICDD 19-0629); ◇ : franklinite (ICDD 22-1012); ▲ : mimetite (ICDD 19-0683); and ? : unidentified
 233 mineral.

234 The Zn, Cu, and Fe arsenates previously observed in this soil (Thouin et al., 2016), adamite ($Zn_2AsO_4(OH)$),
 235 olivenite ($Cu_2AsO_4(OH)$), and pharmacosiderite ($(K,Na,Ba)Fe_4(AsO_4)_3(OH)_5 \cdot 5H_2O$) were again identified in all
 236 samples (Fig.4). Adamite and olivenite are characterized by the same structure so they have similar XRD patterns,
 237 but SEM-EDS showed that crystals were mostly a solid solution of adamite and olivenite (SM4.a). Indeed,
 238 adamite-olivenite crystals were easily recognized because of their prismatic and acicular texture, and the ability to
 239 form large crystals that may grow on grain surfaces. Pharmacosiderite with a cubic structure was also observed
 240 (SM4.b). No evidence of weathering was observed on these arsenate minerals, which were present all along the
 241 soil profile.

242 Mimetite ($Pb_5(AsO_4)_3Cl$), a lead arsenate chloride, was detected exclusively in the water-saturated H4 level at T4
 243 and T8 (Fig.4). Mimetite precipitation was proposed to be part of a soil treatment technology allowing the removal
 244 of arsenate ions from solution (Twidwell et al., 1994 ; Bajda et al., 2006). Indeed, mimetite precipitates under
 245 conditions of low Pb and arsenate concentrations and has a stability domain that covers the pH range of natural

246 waters (Magalhães and Silva 2003; Bajda 2010). Arsenate and chloride ions, which were present in high
247 concentrations in interstitial water throughout the experiment, and the pH range of 5.5-6.0 (Thouin et al., 2017)
248 were optimal for mimetite precipitation. The factor that limited mimetite precipitation in the soil was the low
249 amount of dissolved Pb concentration. Mimetite precipitation in the saturated part of the soil means that Pb was
250 previously released into solution under these conditions; this confirms the hypothesis of progressive dissolution of
251 metal-bearing amorphous phases throughout the experiment. Mimetite was not observed with SEM, but
252 micrometric grains with high lead and other metal concentrations were observed in the saturated depth level
253 (SM4.c). This observation confirms that lead was released and then re-precipitated. Mimetite precipitation,
254 promoted by soil water saturation, was probably one of the phenomena that caused the previously observed
255 immobilization of Pb and As(V). Due to mimetite's broad pH stability range (down to pH = 2), this mineral
256 represents a durable trap for As and Pb. However, the very low dissolved Pb concentration limited mimetite
257 precipitation and relatively high amounts of As remained in solution.

258 **3.2. Modification of the soil organic matter**

259 Characterization of soil OM present in the mesocosm was performed using an elemental flash pyrolyser analyser
260 and Rock-Eval pyrolysis. Results are represented in table 1. Total carbon (C) ranged from 14.7 to 27.8 %, and
261 total hydrogen from 1.6 to 2.4 % in the mesocosm soil. The N content of soil ranged from 0.3 to 0.8 %. TOC
262 ranged between 14.1 and 25.3 %. HI results were low for all mesocosm samples ($< 0.18 \text{ mg HC. g}^{-1} \text{ TOC}$) except
263 for sample H1 – T8. The proportion of O containing OM (OI) ranged between 125 and 200 $\text{mg O}_2. \text{g}^{-1} \text{ TOC}$. All
264 T_{peak} values were higher than 440 °C, and were higher than 500 °C for two samples (H3 – T4 and H4 – T8). The
265 high organic carbon content together with the HI and OI values are quite different from those expected in soil OM
266 (Disnar et al., 2003), but instead show chemical signatures of charcoals (Wolf et al., 2013; Saenger et al., 2015).

267 Previous studies suggest that physical and chemical charcoal properties depend on the temperature of the fire
268 (Schneider et al., 2010; Wolf et al., 2013). Charcoal formation begins with the loss of easily oxidizable OM (such
269 as aliphatic and carboxylic compounds), thus with increasing temperature organic compounds progressively
270 aromatize. High temperature combustion ($> 700^\circ\text{C}$) may cause complete carbonization of OM and may form
271 polyaromatic crystallites or graphite-like structures (Keiluweit et al., 2010). This restructuring of OM is expressed
272 by an increase in TOC and a decrease in OI and HI. Wolf et al., (2013) studied the relationship between charcoal
273 signatures and burning conditions. According to their data, our OM signature (HI/OI, T_{peak}) would correspond to
274 a fire temperature ranging between 300 and 400 °C. However, this temperature seems to be relatively low for

275 melting metals (Fe, Cu, Zn, Pb) from shell parts, thus to form the amorphous phases. Wood was placed on top of
 276 the shell dumps during destruction. The temperature was probably higher in the center of the fire, thus explaining
 277 the difference between the fire temperature signal of charcoal and the total range of temperatures reached during
 278 combustion.

279 **Table 1** Parameters related to OM

| Time | C ^a | H ^a | N ^a | C/N ^a | TOC ^b | T _{peak} ^b | HI ^b | OI ^b | HI/OI ^b |
|--------|----------------|----------------|----------------|------------------|------------------|--------------------------------|-------------------------------|--|--------------------|
| | % | % | % | | % | °C | mg HC. g ⁻¹ TOC | mg O ₂ . g ⁻¹ TOC | |
| H1 | 21.1 | 1.8 | 0.6 | 36.3 | 16.1 | 441 | 13 | 161 | 0.08 |
| H2 | 23.8 | 2.1 | 0.7 | 36.2 | 24.9 | 446 | 11 | 125 | 0.09 |
| H3 | 25.9 | 2.3 | 0.7 | 36.6 | 18.5 | 443 | 17 | 161 | 0.11 |
| H4 | 27.8 | 2.4 | 0.8 | 37.0 | 14.6 | 445 | 15 | 200 | 0.08 |
| H1 | 27.1 | 2.4 | 0.7 | 38.1 | 15.3 | 446 | 15 | 184 | 0.08 |
| H2 | 25.9 | 2.2 | 0.6 | 40.5 | 18.3 | 452 | 16 | 147 | 0.11 |
| H3 | 14.7 | 1.5 | 0.3 | 53.5 | 14.1 | 542 | 18 | 157 | 0.11 |
| H4 | 15.1 | 1.6 | 0.3 | 45.8 | 19.4 | 440 | 14 | 147 | 0.10 |
| H1 | 27.8 | 2.4 | 0.8 | 37.0 | 25.3 | 439 | 37 | 169 | 0.22 |
| H2 | 22.6 | 1.8 | 0.4 | 53.2 | 23.2 | 445 | 16 | 151 | 0.11 |
| H3 | 22.8 | 1.7 | 0.5 | 49.5 | 22.8 | 446 | 18 | 150 | 0.12 |
| H4 | 17.1 | 1.6 | 0.4 | 46.2 | 17.5 | 559 | 18 | 154 | 0.12 |
| Litter | 38.5 | 4.7 | 1.8 | 21.4 | 30.5 | 369 | 268 | 205 | 1.31 |

280 a : Flash pyrolyser analyser; b : Rock-Eval 6

281 The forest litter added at T4 had a very different signal from that of the soil. It has higher organic carbon (30.5 %)
 282 and nitrogen (1.8 %) concentrations, higher HI (268 mg HC. g⁻¹ TOC) and OI (205 mg O₂. g⁻¹ TOC) values, and a
 283 lower T_{peak} (369 °C). Disnar et al. (2003) determined that fresh or fragmented litter normally has high TOC values
 284 (10-40%) and HI values higher than 300 mg HC. g⁻¹ TOC. The T_{peak} of 360-370 °C is mostly attributed to cellulose
 285 and/or lignin, two major components of woody tissues frequently observed in litters. These results confirmed the
 286 immature nature of the organic litter added to the top soil of the mesocosm.

287 The intrinsic OM of the “Place-à-Gaz” soil, with a high C/N and low HI/OI ratio has characteristics of a barely
 288 biodegradable material (Tab.1 and SM5). However, the addition of fragmented forest litter enhanced the proportion
 289 of biodegradable OM in the top soil. The effect of forest litter was visible on surface soil sample H1 – T8, which
 290 had a higher organic carbon content (25.3 %) and a higher HI/OI ratio (0.22; Tab.1 and SM5), but not a higher

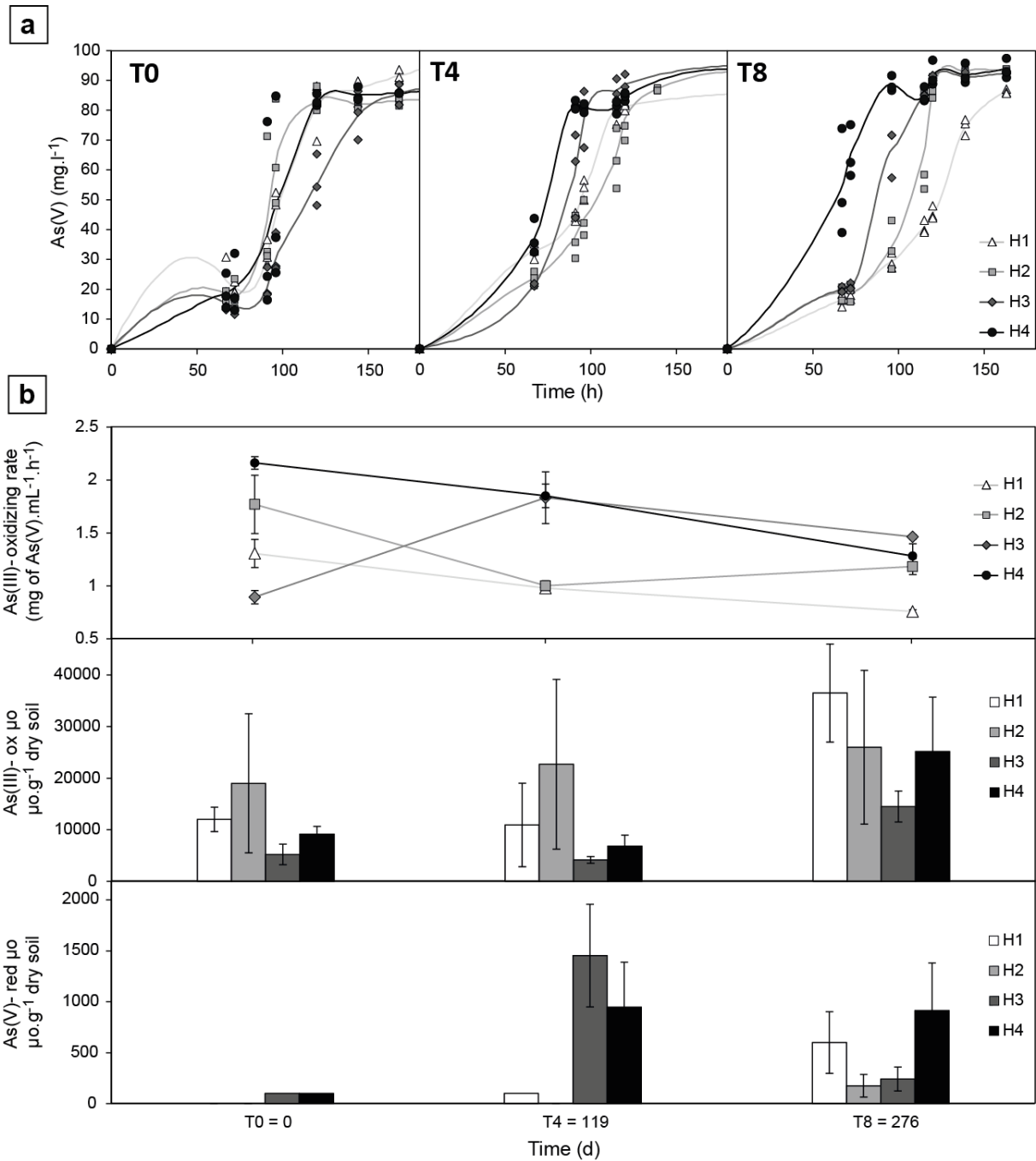
291 C/N ratio. Addition of organic litter increased the carbon mineralization rate in the mesocosm (Thouin et al., 2017),
292 as a result, it was supposed that the addition of litter increased microbial activity.

293 **3.3. Biogeochemistry of arsenic**

294 **Microbial arsenic transformation**

295 As(III)-oxidizing activity tests were used to evaluate the potential for microbial As(III) oxidation during the
296 experiment (Fig. 5). These global activity tests integrate the diversity and abundance of microflora and
297 environmental soil conditions (Lescure et al., 2016). With samples collected at T0, As(III) oxidation started after
298 70 and 90 hours of lapsed time at all levels. The results of microbial As(III) oxidation activity tests at T0 were
299 consistent with results previously obtained with soil sampled from the most polluted zone of the “Place-à-Gaz”
300 site (Thouin et al., 2016), with identical latency of about 100 h. Here, the lapsed time decreased progressively
301 during the mesocosm experiment, particularly in the water-saturated levels. At T8, the As(III) oxidation kinetics
302 of each sample were well separated temporally, with complete As(III) oxidation achieved in time periods that
303 increased as follows: H4 < H3 < H2 < H1. The rate of microbial As(III) oxidation was consistently higher in
304 saturated or alternatively saturated/unsaturated levels H4 and H3 than in unsaturated levels H1 and H2 (except for
305 H3 T0) (Fig.5.b). The rate of microbial As(III) oxidation decreased over time, mostly in H1 and H4, whose As(V)
306 values decrease from 1.3 and 2.2 mg of As(V).mL⁻¹.h⁻¹ at T0 to 0.8 and 1.3 mg of As(V).mL⁻¹.h⁻¹ at T8.

307



308

309 **Fig.5.** Microbial As(III)-oxidizing and As(V)-reducing activities. a: Evolution of As(V) concentration during the
 310 As(III)-oxidizing activity test for the four soil samples at T0, T4 and T8. b: Plot of As(III) oxidation rates
 311 corresponding to the activity tests in "a". Concentration of As(III)-oxidizing and As(V)-reducing microorganisms
 312 evaluated by MPN. Errors bars represent the standard deviation of the mean of three replicates for the four soil
 313 samples. For As(V)-reducing microorganisms a lack of value means that results from the two or three replicates
 314 were < 50 μo.g⁻¹ dry soil. (ox: oxidizing; red: reducing; μo: microorganisms).

315 The evolution of abundance of As(III)-oxidizing and As(V)-reducing microorganisms was followed by MPN
 316 (Fig.5.b). Between T0 and T4, As(III)-oxidizing microorganism concentrations were stable with higher values in
 317 H2 and lower in H3.

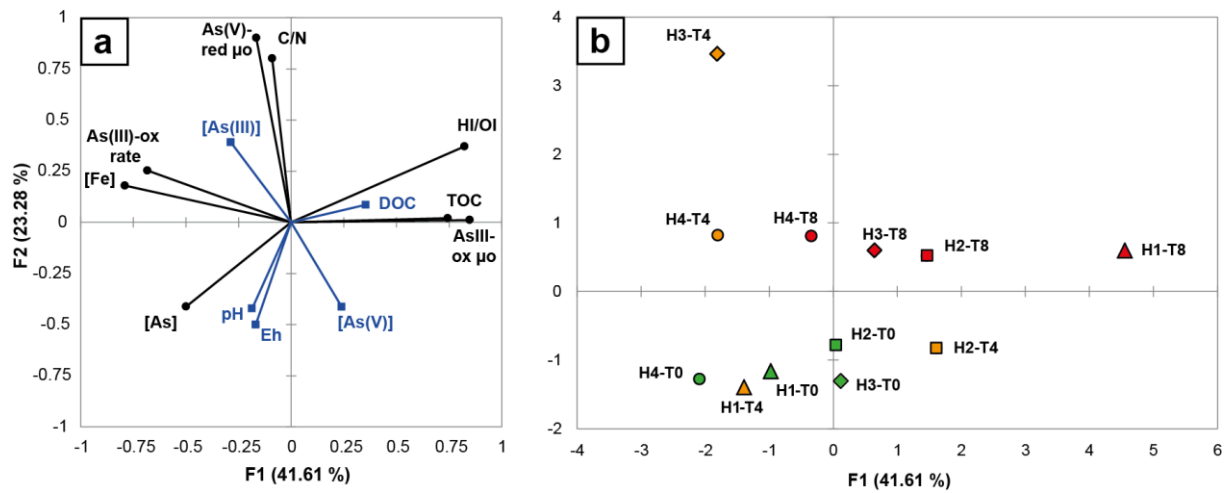
318 After the addition of fragmented forest litter, the concentration of As(III)-oxidizing microorganisms increased in
319 all levels, and particularly in H1. As(V)-reducing microorganisms abundance that could be estimated by the
320 selected MPN method were significantly lower than As(III)-oxidizing microorganisms (one order of magnitude
321 less). At T0, less than 100 As(V)-reducing microorganisms per gram of dry soil were observed. After four (4)
322 months of the experiment, As(V)-reducing microorganism concentrations increased in the saturated and
323 alternatively saturated/unsaturated levels. At T8, the concentration of As(V)-reducing microorganisms increased
324 in H1 and H2, decreased in H3, and remained constant in H4. Thus, both water saturation (for H3 and H4) and
325 OM supply (for H1 and H2) seemed to promote the growth of As(V)-reducing micro-organisms.

326 **Effect of water saturation and addition of litter on arsenic biogeochemical cycle**

327 The impact of water saturation levels and redox oscillation on As solubility has been described in many studies
328 (Kumpiene et al., 2009 ; Weber et al., 2010 ; Parsons et al., 2013 ; Couture et al., 2015) where it was shown that
329 soil saturation increased As solubility by the way of reduction of Fe oxides together with more efficient microbial
330 reduction of As(V). Increased As(III) concentration in soil solution previously observed in the saturated level H4
331 of the mesocosm (Thouin et al., 2017) could be related to increased As(V)-reducing microorganism concentrations
332 in the saturated zones. The stimulation of microbial As(V)-reducing activity induced by soil saturation may have
333 negatively impacted the overall As(III) oxidation rate in water-saturated levels, but could not explain a decreased
334 As(III) oxidation rate in unsaturated levels H1 and H2 (Fig.5.a T8).

335 OM may also affect microbial As(III) oxidizing activity. For example, high concentrations of organic substrates
336 may inhibit this activity (Challan-Belval et al., 2009 ; Bachate et al., 2012 ; Lescure et al., 2016) and may also
337 stimulate aerobic As(V)-reducing activity of soil microorganisms (Yamamura et al., 2009). The As(III) oxidation
338 rate results from the overall activity of all microorganisms involved in As speciation, because microbial As(III)
339 oxidation and As(V) reduction can occur simultaneously, even under aerobic conditions.

340 To describe more precisely the impact of the addition of litter on the available microbial parameters, a principal
341 components analysis (PCA) was built (Fig.6), including variables that describe OM quantities and qualities (TOC,
342 DOC, HI/OI, C/N), microbial As transformation parameters (As(III)-oxidation rate, concentrations of As(III)-
343 oxidizing microorganisms and As(V)-reducing microorganisms), and the variables related to the water phase of
344 the mesocosm, given in Thouin et al., (2017): As speciation and mobility in the interstitial water ([As], [As(III)],
345 [As(V)]), and physicochemical parameters of water (pH, Eh).



346

347 **Fig.6.** PCA using biogeochemical parameters of soil samples (black) with geochemical parameters of soil solutions
 348 (from Thouin *et al.*, 2017) as supplementary data (blue). a: Correlation circle showing variable relationships. b:
 349 Factorial plan showing samples. (ox: oxidizing; red: reducing; μ : microorganisms). Pearson correlation matrix
 350 was presented in SM6.

351 As previously observed, the As(III) oxidation rate seems to be negatively correlated with As(III)-oxidizing
 352 microorganism concentrations ($p = -0.50$) and with DOC ($p = -0.53$) and HI/OI ($p = -0.50$) (Fig.6.a). This
 353 distribution was brought by principal component F1, which represented about 40% of total variability. For this
 354 component, the surface soil (H1-T8), as the end member, is pulled to the right (Fig.6.b) due to the combined effect
 355 of DOC, TOC, HI/OI, and As(III)-oxidizing microorganism concentrations. This level was the most impacted by
 356 the addition of forest litter. The sample distribution along the principal component F1 shows the overall effect of
 357 the litter on the entire mesocosm, with an enhanced influence towards the right from T4 to T8. Moreover, the
 358 distribution of T8 samples clearly depends on their depth because, as previously discussed, the deeper level was
 359 less impacted by the addition of OM.

360 Principal component F2 accounts for 23% of total variability. The concentration of As(V)-reducing
 361 microorganisms and the C/N ratio were correlated ($p = 0.59$) and were the primary contributors to F2. The
 362 previously mentioned positive effect of soil saturation on As(V)-reducing microorganisms is expressed by the
 363 upward translation of samples H3 and H4 between T0 and T4 along the F2 axis (Fig.6.b). Bioavailable OM may
 364 stimulate the As(V)-reducing activity of soil microorganisms under aerobic conditions (Yamamura *et al.*, 2009)
 365 because the As(V)-reducing mechanism linked to the As resistance system consumes energy. In our study,
 366 concentrations of As(V)-reducing microorganisms increased in the non-saturated soil after the addition of
 367 fragmented litter. However, As(V)-reducing microorganisms were correlated to the C/N ratio ($p = 0.59$) but were
 368 not correlated to total OM concentrations (TOC, $p = -0.18$; DOC, $p = -0.09$). The relationship between As(V)-

369 reducing microorganism concentrations in the soil and OM qualities and quantities cannot be confirmed here.
370 Finally, the quantity of As(V)-reducing microorganisms was correlated with As(III) concentrations in soil
371 interstitial water ($p = 0.76$) suggesting that microbial As-reducing activity was promoted by soil saturation.
372 However, the overall proportion of As(III) in interstitial water remained lower than that of As(V) (10 to 20%, Thouin
373 et al., 2017).

374 The present experiment differs from previous studies by two main aspects: (1) the extreme level of metals and As
375 concentrations, that resemble those found in mining wastes (Drewniak et al., 2008) but without the high
376 concentration in sulfur species, and (2) the fact that in spite of water saturation and addition of OM, the redox
377 potential did not reach very low values. Weber et al. (2010) observed a decrease of redox potential down to 0 mV
378 in the porewater of their contaminated surface soil after 20 days of flooding with artificial river water, with a
379 simultaneous strong reduction of As(V), whereas in our experiment, the redox potential always remained higher
380 than +100 mV (Thouin et al., 2017). As a fact, most of the reported studies about redox dynamic were performed
381 with soils or sediments less contaminated than the “Place-à-Gaz” material: 300 ppm As in a polluted floodplain
382 soil (Weber *et al.*, 2010), 375 ppm As in an artificially polluted soil (Couture et al., 2015), 63 ppm As in a
383 contaminated sediment (Moon et al., 2017) compared with 100 000 ppm As in our soil. Thus, the present
384 experiment provides information about microbial As transformation in a biogeochemical environment that was
385 not previously explored in variable redox conditions. Thouin et al. (2016) found that elevated toxic element
386 concentrations (Cu, Pb, Zn, As) seemed to have exerted a selective pressure on the microbial communities, with
387 higher As(III)-oxidizing rates and lower microbial activity involved in carbon mineralization of the microbial
388 populations from the most polluted zone of the site. Thus, phenomena linked to high concentrations of metals and
389 arsenic may have attenuated the decrease of redox potential linked to oxygen consumption in the saturated level,
390 while OM was provided, compared with less polluted environments. Up to now, all As(III)-oxidizing bacteria
391 isolated from soils were heterotrophs or facultative autotrophs (Inskeep et al., 2007; Bachate et al., 2012; Bahar et
392 al., 2013; Dong et al., 2014). The increasing amount of OM and its quality therefore promoted the growth of
393 As(III)-oxidizing microorganisms. However, several studies have shown that elevated concentrations of
394 bioavailable OM negatively impact As(III)-oxidizing bacterial activity (Challan-Belval et al., 2009; Bachate et al.,
395 2012; Lescure et al., 2016). The opposite trend of overall As(III) oxidizing rate with increasing As(III)-oxidizing
396 microorganisms concentration ($p = -0.50$) and with the quality and quantity of OM seems to confirm the inhibiting
397 effect of OM on the specific activity of As(III)-oxidizing microbes. However, globally, As(III) oxidizing
398 microorganisms remained active in presence of OM, even in the saturated zones of the mesocosm, in accordance

399 with the predominance of As(V) in the interstitial water all along the experiment and with the formation of
400 mimetite. This original phenomenon could result from the particular balance between As and OM microbial
401 transformations in the presence of extremely high concentrations of toxic contaminants.

402 **4. Conclusion**

403 The mesocosm experiment provided important information about the mineralogical evolution and stability of As
404 and heavy metal mineral carriers present in the highly-polluted soil at the “Place-à-Gaz” site, as it underwent
405 environmental changes. As, Cu, and Zn-bearing amorphous phases were altered under saturated conditions.
406 Related to this alteration process, SEM results suggest a mechanism of dissolution and re-precipitation of iron in
407 the form of amorphous oxides that may be a secondary sink for As and metals. In contrast, no traces of alteration
408 were observed on crystallized arsenate minerals present in the soil at the beginning of the experiment. However,
409 the formation of mimetite, a lead arsenate chloride mineral, was detected in water saturated zones. This
410 phenomenon contributed to the immobilization of As(V) and Pb, but was limited by the low Pb concentration of
411 the soil solution.

412 The input of OM contributed to the growth of both As(III)-oxidizing and As(V)-reducing microorganisms and
413 negatively impacted the overall As(III) oxidation efficiency. This last phenomenon may be related to both the
414 inhibition of microbial As(III)-oxidizing activities and the development of As(V)-reducing microorganisms.
415 However, As(III)-oxidizing activity remained the major microbial-related phenomenon even in the saturated
416 zones. Altogether, results from the mesocosm experiment show that water saturation of the “Place-à-Gaz” soil
417 during high precipitation episodes is likely to promote the release of Zn and As into the water compartment.
418 However, microbial As(III) oxidation activities, adsorption of As(V) on HFO and precipitation of mimetite are all
419 processes observed during the experiment that contribute to partial immobilization of As, i.e. a decrease of total
420 soluble As. The elucidation of these geochemical and biogeochemical processes at the mesocosm scale will
421 contribute to more precise evaluations of the risks associated with these types of polluted sites and to better design
422 management strategies.

423 **Acknowledgments**

424 This work was co-funded by the Région Centre Val-de-Loire and BRGM (convention 00087485) and the Labex
425 Voltaire (ANR-10-LABX-100-01). The authors wish to thank Philippe Penhoud, Marielle Hatton, and Rachel
426 Boscardin (ISTO) for XRD, CHNS and Rock-Eval results, Pascal Auger (BRGM) for Niton analyses, and Daniel
427 Hube (BRGM) who introduced the environmental issue and provided the polluted material.

428 **References**

- 429 Bachate, S.P., Khapare, R.M., and Kodam, K.M. (2012). Oxidation of arsenite by two β -proteobacteria isolated
430 from soil. *Applied Microbiology and Biotechnology* 93, 2135–2145.
431 DOI: 10.1007/s00253-011-3606-7
- 432 Bahar, M.M., Megharaj, M., and Naidu, R. (2013). Kinetics of arsenite oxidation by *Variovorax* sp. MM-1 isolated
433 from a soil and identification of arsenite oxidase gene. *Journal of Hazardous Materials* 262, 997–1003.
434 DOI: 10.1016/j.jhazmat.2012.11.064
- 435 Bajda, T., Szmít, E., and Manecki, M. (2006). Removal of As (V) from solutions by precipitations of mimetite
436 $Pb_5(AsO_4)_3Cl$. *Environmental Engineering*, 119-124.
- 437 Bajda, T. (2010). Solubility of mimetite $Pb_5(AsO_4)_3Cl$ at 5–55°C. *Environmental Chemistry* 7, 268.
438 DOI: 10.1071/EN10021
- 439 Battaglia-Brunet, F., Dictor, M.-C., Garrido, F., Crouzet, C., Morin, D., Dekeyser, K., Clarens, M., and Baranger,
440 P. (2002). An arsenic(III)-oxidizing bacterial population: selection, characterization, and performance in reactors.
441 *Journal of Applied Microbiology* 93, 656–667.
442 DOI: 10.1046/j.1365-2672.2002.01726.x
- 443 Bausinger, T., and Preuß, J. (2005). Environmental remnants of the First World War: Soil contamination of a
444 burning ground for arsenical Ammunition. *Bulletin of Environmental Contamination and Toxicology* 74, 1045–
445 1053.
446 DOI: 10.1007/s00128-005-0686-z
- 447 Bausinger, T., Bonnaire, E., and Preuß, J. (2007). Exposure assessment of a burning ground for chemical
448 ammunition on the Great War battlefields of Verdun. *Science of The Total Environment* 382, 259–271.
449 DOI: 10.1016/j.scitotenv.2007.04.029
- 450 Challan-Belval, S., Garnier, F., Michel, C., Chautard, S., Breeze, D., and Garrido, F. (2009). Enhancing pozzolana
451 colonization by As(III)-oxidizing bacteria for bioremediation purposes. *Applied Microbiology and Biotechnology*
452 84, 565–573.
453 DOI: 10.1007/s00253-009-2077-6
- 454 Couture, R.-M., Charlet, L., Markelova, E., Madé, B., and Parsons, C.T. (2015). On–Off Mobilization of
455 Contaminants in Soils during Redox Oscillations. *Environmental Science & Technology*. 49, 3015–3023.
456 DOI: 10.1021/es5061879
- 457 Deneele, D (2002). Caractérisation, simulations expérimentales et thermodynamiques de l’altération de déchets
458 vitreux: les scories de première fusion de plomb et de zinc, University Ph.D. Thesis, University of Lille 1, France,
459 2002, 198 pp.
- 460 Disnar, J.R., Guillet, B., Keravis, D., Di-Giovanni, C., and Sebag, D. (2003). Soil organic matter (SOM)
461 characterization by Rock-Eval pyrolysis: scope and limitations. *Organic Geochemistry* 34, 327–343.
462 DOI: 10.1016/S0146-6380(02)00239-5
- 463 Dixit, S., and Hering, J.G. (2003). Comparison of arsenic(V) and arsenic(III) sorption onto iron oxide minerals:
464 implications for arsenic mobility. *Environmental Science and Technology* 37, 4182–4189.
465 DOI: 10.1021/es030309t
- 466 Dong, D., Ohtsuka, T., Dong, D.T., and Amachi, S. (2014). Arsenite oxidation by a facultative
467 chemolithoautotrophic *Sinorhizobium* sp. KGO-5 isolated from arsenic-contaminated soil. *Bioscience,*
468 *Biotechnology, and Biochemistry* 78, 1963–1970.

- 469 DOI: 10.1080/09168451.2014.940276
- 470 Drewniak, L., Matlakowska R., Sklodowska, A. (2008). Arsenite and Arsenate Metabolism of *Sinorhizobium* sp.
471 M14 Living in the Extreme Environment of the Zloty Stok Gold Mine. *Geomicrobiology Journal* 25, 363–370.
472 DOI: 10.1080/01490450802402836
- 473 Drewniak, L., and Sklodowska, A. (2013). Arsenic-transforming microbes and their role in biomining processes.
474 *Environmental Science and Pollution Research* 20, 7728–7739.
475 DOI: 10.1007/s11356-012-1449-0
- 476 Dutra, A.J.B., Paiva, P.R.P., and Tavares, L.M. (2006). Alkaline leaching of zinc from electric arc furnace steel
477 dust. *Minerals Engineering* 19, 478–485.
478 DOI: 10.1016/j.mineng.2005.08.013
- 479 Ettler, V., Komárková, M., Jehlička, J., Coufal, P., Hradil, D., Machovič, V., and Delorme, F. (2004). Leaching of
480 lead metallurgical slag in citric solutions implications for disposal and weathering in soil environments.
481 *Chemosphere* 57, 567–577.
482 DOI: 10.1016/j.chemosphere.2004.07.022
- 483 Inskeep, W. P., Macur, R. E., Hamamura, N. H., Warelow, T. P., Ward, S. A., Santini, J. M. (2007). Detection,
484 diversity and expression of aerobic bacterial arsenite oxidase genes. *Environmental Microbiology* 9, 934-943.
485 DOI: 10.1111/j.1462-2920.2006.01215.x
- 486 Moon, H. S., Kim, B. A., Hyun, S. Y., Lee Y.-H., Shin D. (2017). Effect of the redox dynamics on microbial-
487 mediated As transformation coupled with Fe and S in flow-through sediment columns. *Journal of Hazardous*
488 *Materials* 329, 280-289.
489 DOI: 10.1016/j.jhazmat.2017.01.034
- 490 Juillot, F., Morin, G., Ildefonse, P., Trainor, T.P., Benedetti, M., Galois, L., Calas, G., and Brown, G.E. (2003).
491 Occurrence of Zn/Al hydrotalcite in smelter-impacted soils from northern France: Evidence from EXAFS
492 spectroscopy and chemical extractions. *American Mineralogist* 88, 509–526.
493 DOI: 10.2138/am-2003-0405
- 494 Keiluweit, M., Nico, P.S., Johnson, M.G., and Kleber, M. (2010). Dynamic molecular structure of plant biomass-
495 derived black carbon (biochar). *Environmental Science & Technology* 44, 1247–1253.
496 DOI: 10.1021/es9031419
- 497 Kuai, L., Nair A. A., Polz M. F. (2001) Rapid and simple method for the Most-Probable-Number estimation of
498 arsenic-reducing bacteria. *Applied and Environmental Microbiology* 67, 3168-3173.
499 DOI: 10.1128/AEM.67.7.3168-3173.2001
- 500 Kumpiene, J., Ragnvaldsson, D., Lövgren, L., Tesfalidet, S., Gustavsson, B., Lättström, A., Leffler, P., and
501 Maurice, C. (2009). Impact of water saturation level on arsenic and metal mobility in the Fe-amended soil.
502 *Chemosphere* 74, 206–215.
503 DOI: 10.1016/j.chemosphere.2008.09.068
- 504 Lafargue, E., Marquis, F., and Pillot, D. (1998). Rock-Eval 6 Applications in Hydrocarbon Exploration,
505 Production, and Soil Contamination Studies. *Rev. Inst. Fr. Pét.* 53, 421–437.
506 DOI: 10.2516/ogst:1998036
- 507 Le Forestier, L., Libourel, G. (2008) High temperature behavior of electrostatic precipitator ash from municipal
508 solid waste combustors. *Journal of Hazardous Materials* 154, 373-380.
509 DOI: 10.1016/j.jhazmat.2007.10.034
- 510 Lescure T., Carpentier A., Battaglia-Brunet F., Morel-Desrosiers N.. (2013) Oxidation of As(III) by the Bacterial
511 Community of a Marine Sediment Monitored by Microcalorimetry. *Geomicrobiology Journal* 30, 540-548.

- 512 DOI: 10.1080/01490451.2012.737088
- 513 Lescure, T., Moreau, J., Charles, C., Ben Ali Saanda, T., Thouin, H., Pillas, N., Bauda, P., Lamy, I., and Battaglia-
514 Brunet, F. (2016). Influence of organic matters on AsIII oxidation by the microflora of polluted soils.
515 *Environmental Geochemistry and Health* 38, 911–925.
516 DOI: 10.1007/s10653-015-9771-3
- 517 Magalhães, M.C.F., and Silva, M.C.M. (2003). Stability of lead(II) arsenates. *Monatshefte Für Chemie / Chemical*
518 *Monthly* 134(5), 735–743.
519 DOI: 10.1007/s00706-002-0581-9
- 520 de Mello, J.W.V., Talbott, J.L., Scott, J., Roy, W.R., and Stucki, J.W. (2007). Arsenic speciation in arsenic-rich
521 Brazilian soils from gold mining sites under anaerobic incubation. *Environmental Science and Pollution Research*
522 *- International* 14, 388–396.
523 DOI: 10.1065/espr2006.08.330
- 524 Parsons, C.T., Couture, R.-M., Omeregic, E.O., Bardelli, F., Greneche, J.-M., Roman-Ross, G., and Charlet, L.
525 (2013). The impact of oscillating redox conditions: Arsenic immobilisation in contaminated calcareous floodplain
526 soils. *Environmental Pollution* 178, 254–263.
527 DOI : 10.1016/j.envpol.2013.02.028
- 528 Pisciella, P., Crisucci, S., Karamanov, A., and Pelino, M. (2001). Chemical durability of glasses obtained by
529 vitrification of industrial wastes. *Waste Management* 21, 1–9.
530 DOI: 10.1016/S0956-053X(00)00077-5
- 531 Puziewicz, J., Zainoun, K., and Bril, H. (2007). Primary phases in pyrometallurgical slags from a zinc-smelting
532 waste dump, swietochlowice, upper silesia, poland. *The Canadian Mineralogist* 45, 1189–1200.
533 DOI: 10.2113/gscanmin.45.5.1189
- 534 Saenger, A., Cécillon, L., Poulencard, J., Bureau, F., De Daniéli, S., Gonzalez, J.-M., and Brun, J.-J. (2015).
535 Surveying the carbon pools of mountain soils: A comparison of physical fractionation and Rock-Eval pyrolysis.
536 *Geoderma* 241–242, 279–288.
537 DOI: 10.1016/j.geoderma.2014.12.001
- 538 Schneider, M.P.W., Hilf, M., Vogt, U.F., and Schmidt, M.W.I. (2010). The benzene polycarboxylic acid (BPCA)
539 pattern of wood pyrolyzed between 200°C and 1000°C. *Organic Geochemistry* 41, 1082–1088.
540 DOI: 10.1016/j.orggeochem.2010.07.001
- 541 Seignez, N., Gauthier, A., Bulteel, D., Buatier, M., Recourt, P., Damidot, D., and Potdevin, J.L. (2007). Effect of
542 Pb-rich and Fe-rich entities during alteration of a partially vitrified metallurgical waste. *Journal of Hazardous*
543 *Materials* 149, 418–431.
544 DOI: 10.1016/j.jhazmat.2007.04.007
- 545 Stolz, J., Basu, P., and Oremland, R. (2002). Microbial transformation of elements: the case of arsenic and
546 selenium. *International Microbiology* 5, 201–207.
547 DOI: 10.1007/s10123-002-0091-y
- 548 Swallow, K.C., Hume, D.N., and Morel, F.M.M. (1980). Sorption of copper and lead by hydrous ferric oxide.
549 *Environmental Science and Technology* 14, 1326–1331.
550 DOI: 10.1021/es60171a003
- 551 Thouin, H., Le Forestier, L., Gautret, P., Hube, D., Laperche, V., Dupraz, S., and Battaglia-Brunet, F. (2016).
552 Characterization and mobility of arsenic and heavy metals in soils polluted by the destruction of arsenic-containing
553 shells from the Great War. *Science of The Total Environment* 550, 658–669.

- 554 DOI: 10.1016/j.scitotenv.2016.01.111
- 555 Thouin, H., Battaglia-Brunet, F., Gautret, P., Le Forestier, L., Breeze, D., Séby, F., Norini, M.-P., and Dupraz, S.
556 (2017). Effect of water table variations and input of natural organic matter on the cycles of C and N, and mobility
557 of As, Zn and Cu from a soil impacted by the burning of chemical warfare agents: A mesocosm study. *Science of*
558 *The Total Environment* 595, 279–293.
559 DOI: 10.1016/j.scitotenv.2017.03.218
- 560 Tiedje, J.M., Asuming-Brempong, S., Nüsslein, K., Marsh, T.L., and Flynn, S.J. (1999). Opening the black box of
561 soil microbial diversity. *Applied Soil Ecology* 13, 109–122.
562 DOI: 10.1016/S0929-1393(99)00026-8
- 563 Twidwell, L.G., Plessas, K.O., Comba, P.G., and Dahnke, D.R. (1994). Removal of arsenic from wastewaters and
564 stabilization of arsenic bearing waste solids: Summary of experimental studies. *Journal of Hazardous Materials*
565 36, 69–80.
566 DOI: 10.1016/0304-3894(93)E0054-6
- 567 Weber F. A., Hofacker A. F., Kretzschmar R. (2010). Temperature dependence and coupling of iron and arsenic
568 reduction and release during flooding of a contaminated soil. *Environmental Science and Technology* 44, 116-
569 122.
570 DOI: 10.1021/es902100h
- 571 Vereš, J. (2014). Determination of zinc speciation in metallurgical wastes by various analytical methods.
572 *International Journal*, 5(5).
- 573 Wolf, M., Lehndorff, E., Wiesenberg, G.L.B., Stockhausen, M., Schwark, L., and Amelung, W. (2013). Towards
574 reconstruction of past fire regimes from geochemical analysis of charcoal. *Organic Geochemistry* 55, 11–21.
575 DOI: 10.1016/j.orggeochem.2012.11.002
- 576 Xiao K.-Q., Li L. G., Ma L. P., Zhang S. Y., Bao P., Zhang T., Zhu Y.-G. (2016). Metagenomic analysis revealed
577 highly diverse microbial arsenic metabolism genes in paddy soils with low-arsenic contents. *Environmental*
578 *Pollution* 211, 1-8.
579 DOI: 10.1016/j.envpol.2015.12.023
- 580 Yamamura, S., Watanabe, M., Yamamoto, N., Sei, K., and Ike, M. (2009). Potential for microbially mediated
581 redox transformations and mobilization of arsenic in uncontaminated soils. *Chemosphere* 77, 169–174.
582 DOI: 10.1016/j.chemosphere.2009.07.071
- 583 Zobrist, J., Dowdle, P.R., Davis, J.A., and Oremland, R.S. (2000). Mobilization of arsenite by dissimilatory
584 reduction of adsorbed arsenate. *Environmental Science and Technology* 34, 4747–4753.
585 DOI: 10.1021/es001068h